J. Synchrotron Rad. (1998). **5**, 1215–1221

High-Throughput Asymmetric Double-Crystal Monochromator of the SAXS Beamline at ELETTRA

S. Bernstorff,[a]* H. Amenitsch[b] and P. Laggner[b]

[a]*Sincrotrone Trieste, Strada Statale per Basovizza 14 km 163.5, 34012 Trieste, Italy, and* [b]*Institute for Biophysics and X-ray Structure Research, Austrian Academy of Science, Steyrerg. 17, 8010 Graz, Austria. E-mail: bernstorff@elettra.trieste.it*

(*Received 9 September 1997; accepted 11 December 1997*)

A new high-flux wiggler beamline for fast time-resolved small-angle X-ray scattering (SAXS) based on double-focusing optics has recently commenced operation at the 2 GeV third-generation storage ring ELETTRA at Trieste, Italy. Its non-dispersive double-crystal monochromator contains three pairs of interchangeable asymmetrically cut flat Si(111)-crystal pairs, each of which is optimized for high throughput at one of the three fixed energies 5.4, 8 and 16 keV. To cope with the severe thermal power load produced by a 57-pole wiggler on the first crystal of each pair (up to 5.4 W mm^{-2} and 700 W under normal incidence, for 400 mA), grazing angles of 2° and optimized back-cooling have been chosen. This solution allows simultaneously a gain of 2.5–3.0 in throughput and, accordingly, in flux density. Finite-element analysis as well as commissioning tests showed that the cooling layout functions very satisfactorily, and that up to 5×10^{12} photons s^{-1} are available at the sample (at 8 keV and 250 mA), as predicted.

Keywords: asymmetric crystals; heat loads; optimized cooling layouts; double-crystal monochromators; small-angle X-ray scattering.

1. Introduction

A major problem in operating double-crystal monochromators is the thermal load on the first diffracting crystal surface, which is exposed to the white beam. Perfect Si crystals, which are widely used as X-ray monochromators at synchrotron radiation facilities worldwide, deliver near theoretical performance when illuminated by a low-intensity synchrotron radiation beam (of the order of $\leq$20 W mrad^{-1}). Present day insertion devices at third-generation synchrotron radiation facilities, however, deliver up to 100–1000 times this power. Such high heat loads induce thermal strains that may degrade considerably the monochromator performance or may even damage the crystal if not suitably cooled. To cope with very high heat loads, sophisticated cooling systems are commonly used (*Thermal Management of X-ray Optical Components for Synchrotron Radiation Workshop*, 1994, and references therein) which are based on cryogenic cooling, on crystals having microchannels just below the hot diffracting surface for efficient internal cooling with water or liquid Ga, on cooling with water jets, or on dynamical bending to compensate for thermal crystal deformations.

In this paper we present another approach: at the SAXS beamline each Si(111) crystal will be used at a fixed photon energy only. Thus, small grazing angles of 2° may be chosen, which allows the reduction of the on-surface power density by a factor of the order of 30 compared with normal incidence. Besides spreading the power load over a much larger crystal area, this solution gives simultaneously a gain of the order of 2.5–3.0 in transmitted photon flux and, accordingly, in flux density, with respect to symmetrically cut double-crystal set-ups (Amenitsch, Bernstorff & Laggner, 1995). Due to the strongly reduced power density on the asymmetric crystal surface, a much simpler cooling layout based on thin back-cooled-only crystals now seems feasible, if the water-cooled substrate contains a channel structure suitable for carrying away the still high total absorbed power. This solution also allows the correction for deformations under heat load by prebending the crystals. Design analysis using finite-element methods has been performed for this system, and the crystal behaviour has been tested under heat load. It will be demonstrated that refinements in the heat-flux distribution and in the cooling-channel configuration of the substrate can indeed sufficiently reduce the surface distortion of crystals under high heat loads using back-water-cooling only.

2. Layout of the SAXS beamline

The SAXS beamline (Amenitsch *et al.*, 1997, 1998) has been optimized for time-resolved experiments on fast structural transitions in the submillisecond time region in weakly scattering solutions and partly ordered systems like fibrous and liquid-crystalline materials. At 8 keV, the beamline operates with a SAXS resolution between 10 and 1400 Å in *d*-spacing; simultaneously wide-angle X-ray scattering (WAXS) experiments can be performed between 1.2 and 9.4 Å.

The optical and mechanical layout of the SAXS beamline have been described in detail elsewhere (Amenitsch, Bernstorff & Laggner, 1995). In short, the source is a 4.5 m-long 57-pole permanent-magnet wiggler (Walker, 1989) which emits 3.4 kW mrad^{-2}. The peak magnetic field is 1.55 T, and the critical energy is 4.1 keV. The SAXS beamline accepts up to 1.5×0.3 mrad (horizontal $\times$ vertical) of the wiggler beam. A subsequent C filter and Be windows remove about 50% of the power. But, with ELETTRA operating at 400 mA, still up to 0.7 kW is absorbed by the first monochromator crystal. The thermal power load density would be up to 5.4 W mm^{-2} under normal incidence.

The non-dispersive fixed-exit double-crystal monochromator has three pairs of flat asymmetrically cut Si(111) crystals interchangeable under vacuum. The crystal pairs are optimized (see below) for different discrete and fixed photon energies, namely for 5.4, 8 and 16 keV. As can be seen in Fig. 1, the monochromator consists of four vacuum chambers. Chamber I is located about 18 m after the source point and houses the first crystal of each of the three crystal pairs. Due to geometrical constraints and optical considerations (Amenitsch *et al.*, 1993), we chose to separate the SAXS branch line from the diffraction branch beamline vertically by 1.5 m. Therefore, the second crystals of the three pairs are mounted in three separate chambers (II*a*–II*c*).

To obtain a higher flux density on the sample, a segmented toroidal mirror, situated downstream of the monochromator at about 26.5 m from the source, focuses the X-rays with a demagnification factor of 2.8 both in the horizontal and in the vertical direction onto the fixed detector plane. The sample–detector distance can be adjusted up to a maximum of 3.5 m.

3. Cooling requirements

For considerations of the behaviour of a double-crystal monochromator under heat load, the important quantity is given by the intrinsic angular emittance, ω_h, of the first crystal. It can be described by

$$\omega_h = \omega_s b^{1/2},$$

where ω_s is the intrinsic rocking curve width,

$$b = \sin(\theta_B - \alpha)/\sin(\theta_B + \alpha)$$

is the asymmetry factor, θ_B is the Bragg angle (grazing angle to the reflecting lattice planes), and α is the asymmetry angle (angle between the Bragg planes and the crystal surface). The width of this angular emittance should correspond to the angular acceptance of the second crystal. While ω_s is 7.4 arcsec in the case of Si(111) and 8 keV photon energy, $b^{1/2}$ = 0.23, 0.28 and 0.41 for 5.4, 8 and 16 keV, respectively.

There are three well known effects contributing to a thermally induced mismatch between emittance of the first (hot) and acceptance of the second (cool) crystal, namely overall bending, thermal bump and global lattice expansion. In our case, the overall bending can be neglected because the crystal will be held down to the support on its entire back area by the adhesive force of approximately 0.4 N cm^{-2} produced by the eutectic Ga/In layer which is used for thermal coupling between the crystal and its support. The second contribution, the thermal bump, produces a slope error on the illuminated area of the crystal surface which is given approximately by

$$\omega \simeq 1.43\alpha_{\rm therm} Q D^2/2kA,$$

where $\alpha_{\rm therm}$ is the thermal expansion coefficient, Q is the incoming power, D is the crystal thickness, k is the thermal conductivity and A is the area of the beam footprint on the crystal surface. For a given crystal material and thickness this deformation can be reduced considerably by choosing an asymmetrically cut crystal. The incoming power is then spread over a surface which is increased by a factor of $1/\sin\alpha$, which in turn leads to reduced thermal strains and thus smaller surface slope errors. In Fig. 2, the expected slope error due to the thermal bump is given as a function of the grazing angle $\theta_B - \alpha$. It is compared with the

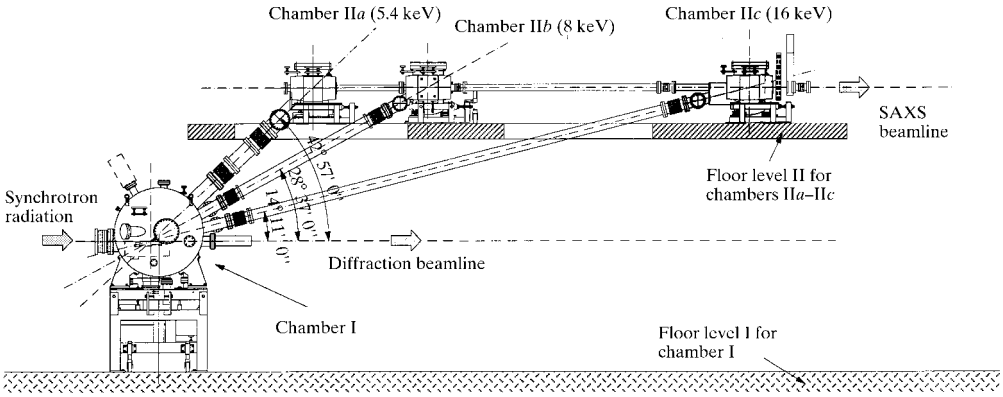

Figure 1
Side view (to scale) of the SAXS double-crystal monochromator consisting of the chambers I and II*a*–II*c*. Each crystal has its own alignment unit allowing for five degrees of freedom. The crystals in chambers II*b* and II*c* can be removed under vacuum from the photon beam path to allow the use of the upstream chambers II*a* and II*b*.

maximum tolerable slope error, which we have chosen to be equal to 25% of the rocking-curve width of the asymmetrically cut Si(111) crystals. From Fig. 2 it follows that only the use of large asymmetry angles, leading to grazing angles of $\leq 2^\circ$, will keep the deformations due to the thermal bump within acceptable limits with our high incoming power load.

The third type of distortion is the global change in the spacing between the crystal lattice planes due to thermal expansion. For a given diffraction angle, this results in a change in the energy of the diffracted photons. Therefore, in a double-crystal monochromator, one of the crystals must be rotated in order to diffract again photons with the same energy as the other crystal. This will result in a vertical variation in the direction of the emerging photon beam. However, for the SAXS monochromator, the exit beam, and thus the crystal angular position, should remain fixed. Then, in order to avoid a noticeable loss in transmitted flux, the temperature difference between the first and second crystal must remain below a certain value, $\Delta T_{\max}$. If we accept, for example, a temperature-induced detuning of the monochromator of 25% of the rocking-curve width $\Delta\theta_R$, which corresponds roughly to an intensity loss of the same order, then $T_{\max}$ is given by

$$T_{\max} = 0.25\Delta\theta_R/\alpha_{\text{therm}} \tan\theta_B = 3.14$$

in the case of 8 keV photon energy. Since this is a very small temperature tolerance, a cooling system had to be chosen which could remove the incoming 700 W very efficiently.

4. Cooling layout and mechanical design of the crystal holder

Since one of the most effective systems for removal of high-power heat loads is the use of microchannels located just underneath the hot surface, we chose to use such a design for the SAXS crystal-cooling support. For this purpose we studied carefully various crystal thicknesses and various cooling-channel geometries, all having a large water/metal interface for enhanced heat exchange capacities, in order to keep the gradients from the crystal surface to the water as small as possible. In these calculations we used a linear-heat model as used in the layout of heat sinks in electronic circuits (Tuckerman & Pease, 1981).

Temperature gradients in a back-cooled crystal scale approximately linearly with the crystal thickness. Therefore, we chose a crystal thickness of only 2.5 mm. For the cooling channels in the crystal support, it turned out that the best performance could be reached with eight U-shaped cooling channels with dimensions of 4×1 mm (depth $\times$ width), separated from each other by 2 mm, which run along the long block side 2 mm below the block surface. For the cooling water, the following parameters were used in the calculations: turbulent water flow with a flow rate of $10.5\,\text{l}\,\text{min}^{-1}$, a pressure difference of 3×10^5 Pa and a 1 K temperature increase between the

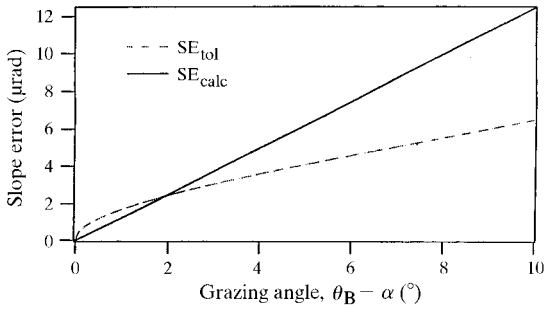

Figure 2
The expected slope error, SE_{calc}, as produced by the thermal bump is given as a function of the grazing angle $\theta_B - \alpha$. It is compared with the maximal tolerable slope error, SE_{tol}, which we have chosen to be 25% of the rocking curve width (at 8 keV photon energy) of the asymmetrically cut Si(111) crystals.

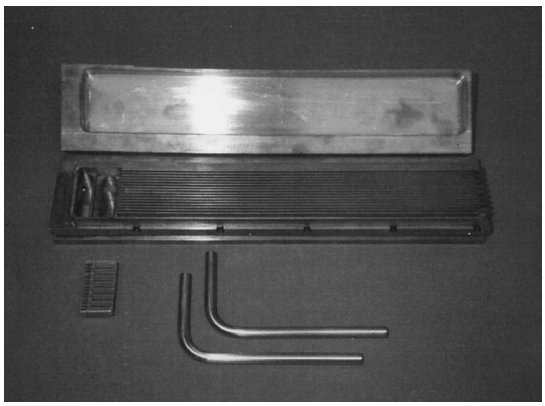

Figure 3
Parts of the crystal support prior to brazing, showing the internal cooling channels machined in the GlidCop base plate, and the stainless-steel water connections.

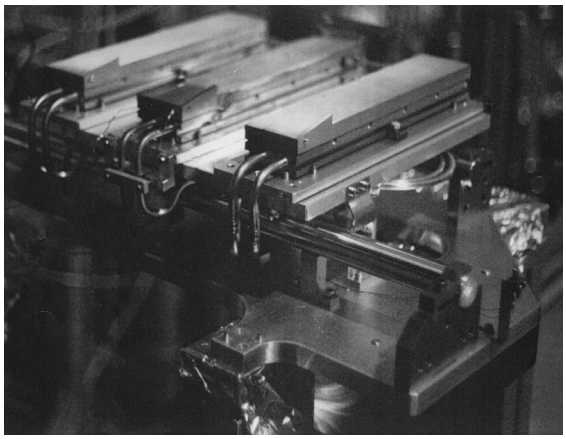

Figure 4
Brazed fully UHV-compatible crystal substrates. The ramps, which can be seen on the front of the cooling blocks, are for protecting the front and the sides of the crystal from accidental exposure (under quasi-normal incidence!) to the synchrotron radiation beam, which might occur during, for example, the initial alignment phase.

water inlet and outlet. Neglecting the thermal resistance of the liquid eutectic In/Ga-alloy layer used to enhance the thermal contact between crystal and cooling block, a total temperature gradient of 8.1 K is expected between the crystal surface and the water inlet.

The first crystal of each pair has a size 38.5 × 195 mm (width × length). The crystals are fixed with their back to the cooling block which consists of a GlidCop top plate, a GlidCop bottom plate having cooling fins, an insert to direct the water flux, and two stainless-steel tubes for the connection to the water supply (see Fig. 3). All these parts are brazed together (see Fig. 4) to avoid any critical vacuum-to-water transitions such as can occur at Viton O-rings or sealings consisting of *e.g.* silicon paste (*i.e.* materials which deteriorate during prolonged exposure to hard X-rays, but which are nevertheless often used in sealing delicate internally water-cooled crystals). After the brazing, the absence of channel occlusion by brazing material, as well as the quality of the brazing connection of each fin to the back plate, have been verified by neutron radiography.

The second crystal of each pair has a size of 50 × 195 mm (width × length). Since the heat load of the monochromatic beam is negligible, no cooling is necessary. Furthermore, a larger thickness of 20 mm could be chosen. This assures a good stability of the crystal shape. The sides of the crystals have indents, which permit them to be clamped strain-free to the crystal holder. No special mounting procedure as in the case of the first crystals (see §6) is required. Vacuum-compatible heating tapes have been attached to the back of the second crystals. These can be used to automatically compensate for variations in the temperature difference between the first and second crystals due to the decrease of the stored electron current with time. Our experience (see §7) showed, however, that it is sufficient to correct manually the pitch of the second crystal slightly (less then 1 arcsec every 4–6 h); thus no sophisticated feedback system is necessary.

5. Performance simulations

To study the effect of the high heat load on the performance of the SAXS crystal monochromator, and to verify the results of our simple linear-heat model calculations for the cooling substrate layout, three-dimensional finite-element analysis (FEA) was performed for our system using the *IDEAS* code (Amenitsch, Hainisch *et al.*, 1995). In Fig. 5 the resulting thermal surface deformations and the corresponding thermal slope errors are shown for the central axis of the crystal surface in the directions parallel and perpendicular to the incoming photon beam, respectively.

According to these FEA calculations, the maximum temperature rise on the crystal surface will be $\Delta T = 6.5$ K, and thus will be slightly higher than the acceptable limit of 3.2 K (see above). The expected slope errors will be up to 12 arcsec sagittally and 6 arcsec tangentially. These deformations are not critical in the sagittal direction, but will be somewhat higher than our acceptable limit in the tangential direction. However, the influence of the eutectic In/Ga layer between crystal and substrate (*i.e.* its holding force and its thermal gradient) was neglected in the calculations. Instead, a fixed coupling between crystal and substrate was assumed, which results in an overestimation of the crystal bending.

6. Crystal mounting procedure

In a double-crystal monochromator the two surfaces must be parallel to within a fraction of their rocking widths in order to be matched for reflection. Since the rocking width between the two asymmetric crystals in the SAXS monochromator is decreased by $b^{-1/2}$ with respect to a symmetric double-crystal monochromator, the Bragg planes have to be parallel to within a few microradians. Furthermore, large

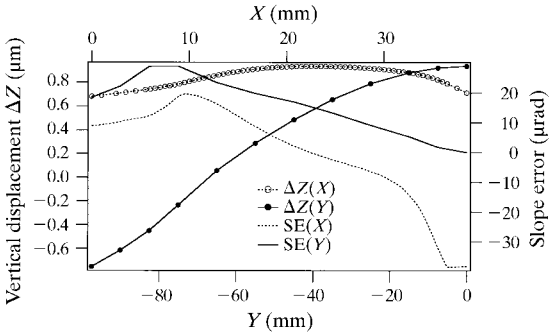

Figure 5
Calculated vertical distortions $\Delta Z(X)$ and $\Delta Z(Y)$ along the central crystal axes perpendicular and parallel to the photon beam direction, respectively. Additionally, the corresponding sagittal and longitudinal slope errors, SE(X) and SE(Y), are shown, respectively. The origin of the coordinate system is on the crystal surface and in the centre of the long crystal side. Only the deformations for one half of the crystal surface are shown, since the deformations on the other half are mirror-symmetric to it.

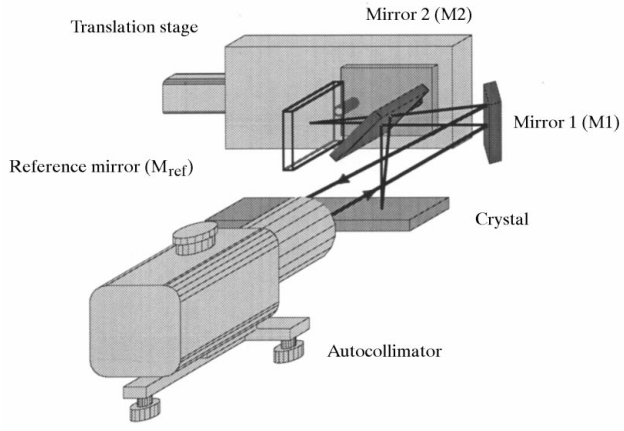

Figure 6
Trace profiler used for *in situ* mounting of the first crystals (see text).

Si crystals having small thicknesses of 2.5 mm or less deform easily. This means that great care has to be taken to mount crystals as stress-free as possible. It might be for that reason that up to now asymmetric double-crystal monochromators have not been in routine use at high-flux beamlines.

For facilitating the mounting procedure of the crystals we used *in situ* a long-trace profiler, which is shown schematically in Fig. 6. It consists of a combination of an autocollimator (DA80 dual-axis from Rank Taylor Hobson Ltd), a translation stage (Newport Micro Control, 1 μm step width) and three mirrors. The autocollimator was placed in front of the open monochromator vessel (diameter 0.9 m). Inside the vessel we mounted temporarily the fixed mirror M1, as well as the translation stage with the mirrors M2 and M_{ref}. Using mirrors M1 and M2 the crystal surface could be sampled along the beam direction, and thus local angular deviations from the ideal plane could be detected with a resolution of 0.1 arcsec. Height profiles of the crystal surface were obtained by integrating the experimental slope data. Errors due to imperfections in the slide were found to be absolutely reproducible, and could be eliminated by subtracting reference measurements obtained using M_{ref} in normal incidence while moving the translation stage over the same range used for the crystal measurements.

Since we found that a better planarity of the crystals can be obtained if clamping to the cooled GlidCop substrate is avoided, the crystals are held only by the adhesive forces due to the eutectic GaIn layer. In Fig. 7 a typical example of a slope and height profile is shown for the 8 keV crystal. The height profile is very smooth, as is to be expected from a polished surface, but shows small local deformations caused by a non-homogeneous eutectic layer thickness and also by minor deviations from a perfect surface flatness of the stress-free crystal. The measured slope errors are between 2 and 15 arcsec. This clearly lies over the random-noise error limit of our long-trace-profiler set-up, so that errors due to air turbulence or thermal effects could be neglected.

7. Experimental results

The monochromator performance under heat load was measured by rotating the second crystal with a mechanical resolution of 0.1 arcsec. A calibrated Si photodiode with an active area of 1 cm^2 was used to determine the absolute photon flux after the monochromator. The heat load on the crystal varied linearly with the stored electron current, and could also be controlled by changing the wiggler gap or by using less then three segments. The illuminated area could be varied using water-cooled slit systems. The cooling-water flow rate in the substrate was varied from 1 to 15 l min^{-1}.

Initially, even under very low power loading, the rocking curves showed that the first crystal was so much distorted that it was only marginally useful as an X-ray monochromator. After the crystal had been mounted more carefully using the long-trace profiler *in situ* to minimize mechanical deformations, the performance of the monochromator improved considerably. Fig. 8 shows a set of rocking curves, which were obtained under 440 W heat load and at different cooling-water flow rates. The central minimum which can be seen in all rocking curves was still due to mechanical deformations created during mounting. As shown in Fig. 9, the angular position of these rocking curves remains constant for high flow rates, whereas it shifts to lower values for smaller flow rates. From the shift in peak position of these rocking curves, it follows that flow rates of at least 10.5 l min^{-1} are needed to keep the increase of the temperature of the first crystal surface below 3–4 K, as was predicted by the finite-element analysis.

However, contrary to what one would expect, for high flow rates the peak intensity reduces slightly, and the width of the rocking curves become larger. This is because for flow rates above about 10 l min^{-1} (corresponding to water pressures above 5×10^5 Pa), the surface of the crystal substrate started bending. These effects, however, could be minimized by prebending the crystals to a slightly concave shape during mounting. For this, the thickness of the eutectic layer was varied by adding small stripes of indium with the appropriate thickness where necessary. Thus, the residual slope errors in working condition (full power load

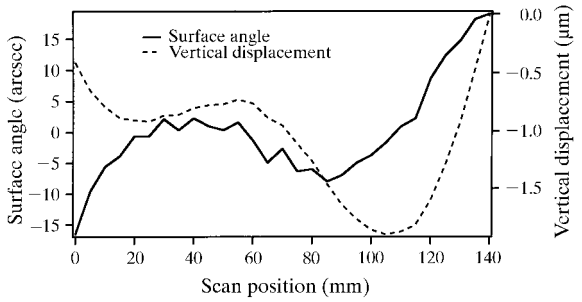

Figure 7
Long-trace profiler scan of the 8 keV Si(111) crystal showing residual slope and height variations after subtraction of the reference scan data.

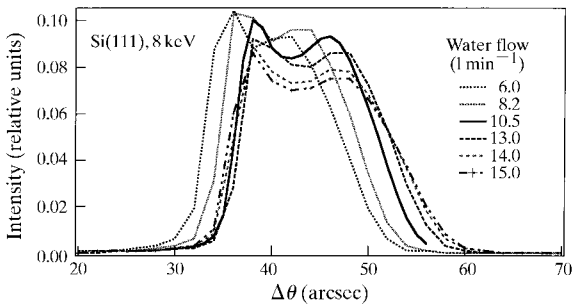

Figure 8
Si(111) rocking curves measured at different cooling-water flow rates. The photon energy was 8 keV and the absorbed heat load was 440 W.

and high water pressure) can easily be made smaller than the required 2 arcsec (see §3) and thus can become fully acceptable. Our experience shows that the stability of this kind of mounting is >0.5 years.

After the cooling system had been optimized, we measured the performance values of the SAXS beamline and compared them with calculated values (Amenitsch, Bernstorff & Laggner, 1995) which we had obtained using the ray-tracing program *SHADOW* (Welnak *et al.*, 1994). Focal spot sizes were determined using a gas-filled Gabriel-type detector (Gabriel, 1977; Mio *et al.*, 1997). The measured spot dimensions of 1.5×0.6 mm (horizontal × vertical) compare very well with the theoretical values, 1.4×0.6 mm. With the photodiode we determined in the focus a total flux of 2×10^{12} photons s^{-1} with a flux density of 4.5×10^{11} photons s^{-1} mm^{-2} (8 keV, at 250 mA). These are close to the calculated values of 5×10^{12} photons s^{-1} and 5×10^{11} photons s^{-1} mm^{-2}, respectively. In Fig. 10 a typical rocking curve for 8 keV photon energy is shown with a FWHM of only 4.2 arcsec, as predicted by ray-tracing calculations. From it a spectral resolution of 0.5×10^{-3} has been evaluated. The large vertical separation of 1.5 m between the incoming and monochromatic beam gives a very low parasitic background in the camera. For the nominal acceptance values [1 × 0.3 mrad (horizontal × vertical)] SAXS resolutions up to 1400 × 400 Å have been achieved.

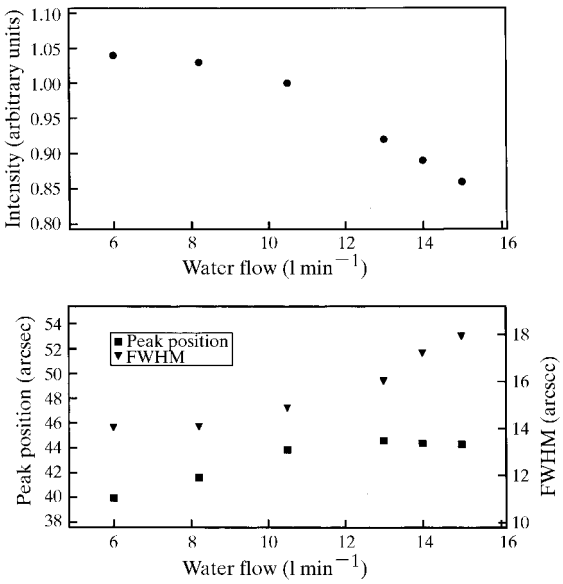

Figure 9
Influence of the cooling-water flow on the intensity, position and FWHM of the Si(111) rocking curve from Fig. 8.

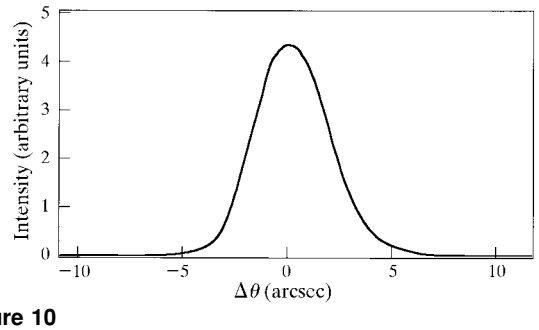

Figure 10
Typical rocking curve of the monochromator, for 8 keV photons.

8. Concluding remarks

The cooling layout for the crystals in the asymmetric double-crystal monochromator of the SAXS beamline has been presented. The optical mounting technique described allows large thin crystals to be mounted sufficiently stress-free with micrometre precision with the flatness required over their entire surface area. It has been demonstrated by finite-element analysis as well as by experimental tests under heat load that the performance of thin strongly asymmetrically cut Si(111) crystals, in combination with back-cooling by means of a water-cooled substrate, is sufficient to cope with the high power delivered by the wiggler source if an adequate cooling support structure is chosen. Therefore, for the SAXS beamline at ELETTRA this conventional cooling layout has been chosen for its greater manufacturing and usage ease, reliability and lower costs.

The usefulness of the presented cooling design for high-power loads is not restricted to fixed-energy monochromator systems. It could also be an interesting alternative to more sophisticated cooling schemes in certain tunable double-crystal monochromators, where, by a suitable choice of the crystal movements and cuts, the grazing angle on the first crystal surface can be kept small throughout the whole tuning range. Examples of such monochromators with adjustable asymmetry have been proposed already at the ESRF (Comin, 1990), and built and tested at the APS (Smither & Fernandez, 1994): here, grazing angles on the first crystal surface can be kept small by rotating asymmetrically cut crystals around an axis perpendicular to the diffraction planes during energy scanning.

The authors would like to thank A. Gambitta for valuable discussions, and B. Hainisch for performing the finite-element heat-load calculations with *IDEAS*.

References

Amenitsch, H., Bernstorff, S., Kriechbaum, M., Lombardo, D., Mio, H., Rappolt, M. & Laggner, P. (1997). *J. Appl. Cryst.* **30**, 872–876.
Amenitsch, H., Bernstorff, S. & Laggner, P. (1993). Internal Report ST/S-R-93/07. Sincrotrone Trieste, Trieste, Italy.
Amenitsch, H., Bernstorff, S. & Laggner, P. (1995). *Rev. Sci. Instrum.* **66**, 1624–1626.
Amenitsch, H., Bernstorff, S., Rappolt, M., Kriechbaum, M., Mio, H. & Laggner, P. (1998). *J. Synchrotron Rad.* **5**, 506–508.

Amenitsch, H., Hainisch, B., Laggner, P. & Bernstorff, S. (1995). *Synchrotron Rad. News*, **8**, 22–27.
Comin, F. (1990). ESRF Internal Report Exp/FC/90/01. ESRF, Grenoble, France.
Gabriel, A. (1977). *Rev. Sci. Instrum.* **48**, 1303–1305.
Mio, H., Chemloul, M., Laggner, P., Amenitsch, H., Bernstorff, S. & Rappolt, M. (1997). *Nucl. Instrum. Methods*, A**392**, 384–391.
Smither, R. K. & Fernandez, P. B. (1994). *Nucl. Instrum. Methods*, A**347**, 313–319.
Thermal Management of X-ray Optical Components for Synchrotron Radiation Workshop (1994). Argonne National Laboratory, Argonne, Illinois, USA.
Tuckerman, D. B. & Pease, R. F. W. (1981). *IEEE Electron Device Lett.* **2**(5), 126.
Walker, R. P. (1989). *Radiation Sources. Conceptual Design for ELETTRA*. Sincrotrone Trieste, Trieste, Italy.
Welnak, C., Chen, G. J. & Cerrina, F. (1994). *Nucl. Instrum. Methods*, A**347**, 344–347.